

Optimization of steady suction for disturbance control on infinite swept wings

Jan O. Pralits^{a)}

Department of Mechanics, KTH, SE-100 44 Stockholm, Sweden

Ardeshir Hanifi

Swedish Defence Research Agency, FOI, Aeronautics Division, FFA, SE-172 90 Stockholm, Sweden

(Received 27 November 2002; accepted 12 June 2003; published 5 August 2003)

We present a theory for computing the optimal steady suction distribution to suppress convectively unstable disturbances in growing boundary layers on infinite swept wings. This work includes optimization based on minimizing the disturbance kinetic energy and the integral of the shape factor. Further, a suction distribution in a continuous control domain is compared to an approach using a number of discrete pressure chambers. In the latter case, the internal static pressures of these chambers are optimized. Optimality systems are derived using Lagrange multipliers. The corresponding optimality conditions are evaluated using the adjoint of the parabolized stability equations and the adjoint of the boundary layer equations. Results are presented for an airfoil designed for medium range commercial aircraft. We show that an optimal suction distribution based on a minimization of the integral of the shape factor is not always successful in the sense of delaying laminar-turbulent transition. It is also demonstrated that including different types of disturbances, e.g., Tollmien–Schlichting and cross-flow types, in the analysis may be crucial. © 2003 American Institute of Physics. [DOI: 10.1063/1.1597684]

I. INTRODUCTION

Reducing the viscous drag on a wing while maintaining operational properties such as lift for example, is of great interest and the research in this area is vast.¹ It is known that the viscous drag increases dramatically as the boundary layer flow changes from a laminar to a turbulent state. Therefore, a decrease in drag can be seen as increasing the laminar portion of the wing, or moving the point of laminar-turbulent transition downstream. Transition in the boundary layer on aircraft wings is usually caused by breakdown of small disturbances which grow as they propagate downstream. The growth of these disturbances can be analyzed using linear stability theory in which it is assumed that perturbations with infinitely small amplitude are superposed on the laminar mean flow. The growth rate can then be used to predict the transition location using the so-called e^N method.^{2,3} Here it is assumed that transition will occur at the location where the total amplification of the disturbance, with respect to the first streamwise position where the disturbance starts to grow, attains an empirically determined value, whose logarithm is generally denoted by N .

The stabilization effect of steady boundary layer suction on disturbance growth is well known⁴ and has been utilized for laminar flow control, for an extensive review see Joslin.¹ However, in most cases the design of suction distributions relies on the experience of the engineer which may not always give the optimal solution, i.e., to give the largest delay

of laminar-turbulence transition at a given suction power. In the last 10 years, the development of optimal control theory and its application to fluid mechanics problems has been rapid and a number of attempts have been made to optimize the steady suction distribution in order to control the growth of disturbances, e.g., Hill,⁵ Balakumar and Hall,⁶ Cathalifaud and Luchini,⁷ Pralits *et al.*,⁸ Airiau *et al.*⁹ In all of these works the optimization methods are gradient based and utilize the potential of adjoint methods to obtain the gradients of interest. Other investigations including those by Mughal,¹⁰ Walther *et al.*,¹¹ Högberg and Henningson¹² consider unsteady suction/blowing. This approach may not be suitable for flow control on aircraft wings at the present time¹³ due to the complexity of its implementation. A common approach in these works^{6–9} is to minimize some measure of the disturbance growth, either the disturbance kinetic energy^{7–9} or the N -factor.⁶ Airiau *et al.*,⁹ in contrast to the others, did also try to minimize the shape factor which for 2D disturbances in a 2D boundary layer should result in a suppression of disturbance amplification. Minimizing the shape factor is a more heuristic approach based on the knowledge that in such flows the two-dimensional disturbances are stabilized by any thinning of the boundary layer. Their results showed that an optimal suction distribution based on minimizing the shape factor does have a damping effect on the disturbance growth. The advantage of this approach is that only one state equation has to be solved which saves computational time. A negative aspect of not explicitly minimizing a measure of the disturbances is that one cannot know if the computed suction distribution will have a damping effect on the disturbances.

^{a)}Also at Swedish Defense Research Agency, FOI, Aeronautics Division, FFA, SE-172 90 Stockholm, Sweden. Electronic mail: jan.pralits@mech.kth.se

This has to be calculated afterwards, once the optimal suction distribution is obtained.

In Pralits *et al.*⁸ the idea of multidisturbance control was introduced. The reason behind it is that, for certain types of flows, it is not clear which types of disturbances will be dominant in terms of amplification. An example is the Blasius flow in which, depending on the initial amplitudes, either two-dimensional Tollmien–Schlichting (TS) waves or streamwise streaks grow the most. In three-dimensional boundary layers on wings there is usually a streamwise region close to the leading edge with a strong negative pressure gradient, where cross-flow waves are the most amplified disturbances. Further downstream, where the pressure gradient is zero or positive, TS waves are the most amplified ones. When computing an optimal suction distribution it is also necessary to make sure that the mean flow modification due to a computed suction distribution for a specific disturbance does not trigger the growth of other disturbances.

In real applications, steady boundary layer suction is usually done using a number of discrete pressure chambers (see, e.g., Reneaux and Blanchard,¹⁴ Ellis and Poll,¹⁵ Preist and Paluch,¹⁶ Bieler and Preist,¹⁷ Joslin¹). In such cases, the suction velocity is a function of the surface porosity, hole geometry and the pressure difference between the pressure distribution on the wing and static pressure in the chambers.^{16,17} This means that the size, position and the internal static pressure of each chamber are the design variables. The suction distribution is then given by the specific choice of these parameters. Atkin¹⁸ used an engineering approach to design of the suction system in which he utilized the stability characteristics of the flow. Here, the static pressure in the pressure chambers, based on an automatized trial and error technique, were chosen such that the amplification of disturbances stayed under a specified value.

Most of the previous works^{6–9} on optimal steady suction deal with incompressible boundary layer flows on flat plates. Hill⁵ analyzed an infinite swept wing for inverse design of laminar boundary layers but no details were given of how this was done. The considered suction distributions have been applied in a continuous^{6–9} or a number of discrete control domains.⁹ However, so far no study has shown how to incorporate the use of pressure chambers in order to approach a real application.

In this paper we extend the work by Pralits *et al.*,⁸ to compressible boundary flows on infinite swept wings. Here we compare the case of minimizing the disturbance kinetic energy with the simplified approach⁹ of minimizing the integral of the shape factor. The feasibility of the control is addressed by comparing two different ways of computing the suction distribution: a continuous distribution of mass flux on the wall in a control domain, and a number of discrete pressure chambers, which constitutes a more realistic approach to obtaining a suction distribution on the wall. The evolution of disturbances is analyzed using the parabolized stability equations (PSE) (see Bertolotti *et al.*,¹⁹ Malik and Balakumar,²⁰ Simen,²¹ Herbert²²), and the laminar mean flow is computed using the two-dimensional three-component boundary layer equations (BLE). We use optimal control theory, in which the aim is to minimize a given objective

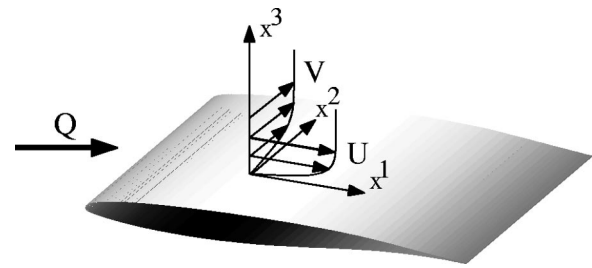


FIG. 1. Definition of the coordinates for the infinite swept wing.

function with state equations and the control energy as constraints. The problem is solved using a Lagrange multiplier technique, which yields an optimality system consisting of state and corresponding adjoint equations from which an optimality condition is evaluated. Here, we couple the adjoint of the PSE with the adjoint of the boundary-layer equations in order to find the optimality condition. The derivation of the optimality system is similar to that presented in Pralits *et al.*⁸ and is therefore presented here in a more compact form. Results are presented for control of disturbance growth in a boundary layer on a wing designed for commercial aircraft.

II. PROBLEM FORMULATION

The flow field considered here is the boundary layer on a swept wing with infinite span which is obtained by solving the mass, momentum, and energy conservation equations for a viscous compressible fluid. The equations are written in an orthogonal curvilinear coordinate system with streamwise, spanwise, and wall-normal coordinates denoted as x^1 , x^2 , and x^3 , respectively, see Fig. 1. A length element is defined as $ds^2 = (h_1 dx^1)^2 + (h_2 dx^2)^2 + (h_3 dx^3)^2$ where h_i is the scale factor. The total flow field, q_{tot} is decomposed into a mean, \bar{q} , and a perturbation part, \tilde{q} , as

$$q_{\text{tot}}(x^1, x^2, x^3, t) = \bar{q}(x^1, x^3) + \tilde{q}(x^1, x^2, x^3, t),$$

where $\bar{q} \in [U, V, W, P, T, \rho]$ and $\tilde{q} \in [\tilde{u}, \tilde{v}, \tilde{w}, \tilde{p}, \tilde{T}, \tilde{\rho}]$. Here U , V , W are the streamwise, spanwise and wall-normal velocity components of the mean flow, respectively, T is the temperature, ρ the density, and P the pressure. The respective lower case variables correspond to the disturbance quantities. The equations are derived for a quasi-three-dimensional mean flow with zero variation in the spanwise direction. The evolution of convectively unstable disturbances is analyzed in the framework of the nonlocal stability theory. The mean flow and disturbance equations in the following sections are given in dimensionless form. All flow and material quantities are made dimensionless with the corresponding reference flow quantities at a fixed streamwise position x_0^* , except the pressure, which is referred to twice the corresponding dynamic pressure. Here, dimensional quantities are denoted by the superscript \star .

The reference length scale is taken as $l_0^* = (\nu_0^* x_0^* / U_0^*)^{1/2}$. The Reynolds and Mach number are defined as $\text{Re} = l_0^* U_0^* / \nu_0^*$ and $M = U_0^* / (\mathcal{R} \gamma T_0^*)^{1/2}$, respectively, where \mathcal{R} is the specific gas constant, ν the kinematic viscosity, and

γ the ratio of the specific heats. In the proceeding sections the scale factors $h_2, h_3 = 1$ are due to the infinite swept wing assumption.

A. Mean-flow equations

The dimensionless boundary layer equations (BLE) written in primitive variable form can be seen in Appendix A and are here written in symbolic form as

$$L_B \mathbf{Q} = 0, \quad (1)$$

where $\mathbf{Q} = (U, V, W, T)^T$. The suction distribution is imposed using the wall normal velocity component at the wall $W_w(x^1) = W(x^1, 0)$. Non-slip conditions are applied to the other velocity components and we assume an adiabatic wall condition for the temperature. Equation (1) is integrated from the stagnation point in the downstream direction normal to the leading edge. Note that for the boundary layer approximation to be valid, the wall normal velocity at the wall, W_w , should be of $O(\text{Re}^{-1})$. Here, it is assumed that the pressure distribution on the airfoil does not change as the suction distribution is applied. If the suction distribution would result in a large change in the boundary layer thickness, then it might be necessary to update the pressure distribution in the optimization process.

B. Disturbance equations

The perturbations are assumed to be time and spanwise periodic waves as

$$\tilde{\mathbf{q}}(x^i, t) = \hat{\mathbf{q}}(x^1, x^3) \Theta,$$

where

$$\Theta = \exp\left(i \int_{X_0}^{x^1} \alpha(x') dx' + i\beta x^2 - i\omega t\right). \quad (2)$$

Here α is the complex streamwise wave number, β the real spanwise wave number and ω the real disturbance angular frequency. X_0 is the initial streamwise position where the disturbances are superimposed on the mean flow. We assume a scale separation Re^{-1} between the weak variation in the x^1 direction and the strong variation in the x^3 direction. Further, it is assumed that $\partial/\partial x^1 \sim O(\text{Re}^{-1})$ and $W \sim O(\text{Re}^{-1})$. Introducing the ansatz given by Eq. (2) and the assumptions above in the linearized governing equations, yields a set of nearly parabolic partial differential equations.^{19–22} The system of equations, denoted parabolized stability equations (PSE), can be seen in Appendix A and are here written in symbolic form as

$$L_P \hat{\mathbf{q}} = 0, \quad (3)$$

where $\hat{\mathbf{q}} = (\hat{\rho}, \hat{u}, \hat{v}, \hat{w}, \hat{T})^T$. Here $\hat{u}, \hat{v}, \hat{w}$, and \hat{T} are subject to Dirichlet boundary conditions. To remove the ambiguity of having x^1 dependence of both the amplitude and wave function in the ansatz, and to maintain a slow streamwise variation of the amplitude function $\hat{\mathbf{q}}$, a so-called auxiliary condition is introduced

$$\int_0^{+\infty} \hat{\mathbf{q}}^H \frac{\partial \hat{\mathbf{q}}}{\partial x^1} dx^3 = 0, \quad (4)$$

where superscript H denotes the complex conjugate transpose. Equation (3) is integrated in the downstream direction normal to the leading edge with an initial condition given by local stability theory. At each x^1 position the streamwise wave number α is iterated such that the condition given by Eq. (4) is satisfied. After a converged streamwise wave number has been obtained, the growth rate of the disturbance kinetic energy can be calculated from the following relation:

$$\sigma = -\alpha_i + \frac{\partial}{\partial x^1} (\ln \sqrt{E}),$$

where

$$E = \int_0^{+\infty} \rho (|\hat{u}|^2 + |\hat{v}|^2 + |\hat{w}|^2) dx^3.$$

The growth rate can then be used to predict the transition location using the so-called e^N method.^{2,3} The N -factor based on the disturbance kinetic energy is given as

$$N_E = \int_{X_{n1}}^X \sigma dx^1,$$

where X_{n1} is the lower branch of the neutral curve. A complete description of Eq. (3) is found in Pralits *et al.*,²³ and corresponding numerical schemes used here are given in Hanifi *et al.*²⁴

III. OPTIMAL CONTROL

The approach of the current work is to use optimal control theory to find the optimal mean flow suction distribution in order to suppress the growth of convectively unstable disturbances. In this paper we investigate different control variables and objective functions. First, a general introduction is given in this section. Then follows a concise description of the Lagrange multiplier technique applied to the problem of minimizing a measure of the disturbances using the mass flux on the wall ($\dot{m}_w = W_w \rho_w$) as control variable.

The problem consists of the state variables \mathbf{Q} and $\tilde{\mathbf{q}}$; a control variable given by the mass flux on the wall; constraints on the state variables given by the BLE and PSE; and an objective function, a measure of the state, to be minimized.

The final goal of boundary-layer suction is to increase the laminar portion of the wing, i.e., to move the location of laminar-turbulent transition further downstream, and thus decrease the viscous drag. It is therefore important that the chosen objective function can be related to the transition process. One choice is to measure the kinetic energy of a certain disturbance at a downstream position, say X_f . This can be written as

$$E_f = \frac{1}{2} \int_{Z_0}^{Z_1} \int_0^{+\infty} \tilde{\mathbf{q}}^H M \tilde{\mathbf{q}} h_1 dx^2 dx^3, \quad (5)$$

where $M_k = \text{diag}(0, 1, 1, 1, 0)$ which means that the disturbance kinetic energy is calculated from the disturbance velocity components. Hanifi *et al.*²⁵ used a measure which also included $\hat{\rho}$ and \hat{T} . If the position X_f is chosen as the upper branch of the neutral curve, then the measure can be related

to the maximum value of the N factor.⁹ If in addition, the value of the N factor of the measured disturbance is the one which first (with zero control) reaches the transition N factor, then the position can be related to the onset of laminar-turbulent transition. It is, however, not clear, *a priori*, that such a measure will damp the chosen disturbance or other ones in the whole unstable region, especially if different types of disturbances are present, such as TS and cross-flow waves. For Blasius flow, it has been shown that an objective function based on a single TS wave is sufficient to successfully damp the growth of other TS waves.^{8,9} On a wing however, it is common that both TS and cross-flow waves are present. An alternative is therefore to measure the kinetic energy as the streamwise integral over a defined domain. Using such an approach several different disturbances, with respective maximum growth rate at different positions, can be accounted for in the same domain. Here, the size of K disturbances superimposed on the mean flow at an upstream position X_0 , is measured by their total kinetic energy as

$$E_\Omega = \sum_{k=1}^K \frac{1}{2} \int_{X_{ms}}^{X_{me}} \int_{Z_0}^{Z_1} \int_0^{+\infty} \tilde{\mathbf{q}}_k^H M_k \tilde{\mathbf{q}}_k h_1 dx^1 dx^2 dx^3. \quad (6)$$

We now define the objective function based on the disturbance growth as

$$\mathcal{J}_0 = \xi E_\Omega + (1 - \xi) E_f, \quad (7)$$

where the parameter ξ can be chosen between zero and one, depending on the quantity one wants to minimize. In order to have a well-posed problem, the control needs to be bounded. This is done by quantifying the control effort as

$$E_C = \int_{X_{cs}}^{X_{ce}} \dot{m}_w^2 h_1 dx^1. \quad (8)$$

This measure has a physical meaning and also enables comparison of efficiency of different objective functions. Taking the square of \dot{m}_w means that both blowing and suction will be accounted for in E_C .

A concise description of the objective can now be made: find the control \dot{m}_w , and corresponding states \mathbf{Q} and $\tilde{\mathbf{q}}$ which minimizes the objective function \mathcal{J}_0 with the constraints given by Eqs. (1), (3), (4), and (8). We now use a Lagrange multiplier technique to replace the original constrained problem with an unconstrained one, see, e.g., Gunzburger.²⁶ In order to enforce the constraints we introduce the adjoint variables \mathbf{Q}^* , \mathbf{q}^* , r^* , λ^* , χ^* and the Lagrangian functional

$$\mathcal{L} = \mathcal{J}_0 - \mathcal{J}_1, \quad (9)$$

where

$$\begin{aligned} \mathcal{J}_1 = & \langle \mathbf{Q}^*, L_B \mathbf{Q} \rangle + \int_{X_{cs}}^{X_{ce}} \lambda^* [\dot{m}(x^1, 0) - \dot{m}_w] h_1 dx^1 + \chi^* \left(E_C \right. \\ & \left. - \int_{X_{cs}}^{X_{ce}} \dot{m}_w^2 h_1 dx^1 \right) + \langle \mathbf{q}^*, L_P \hat{\mathbf{q}} \rangle + \left\langle r^* \hat{\mathbf{q}}, \frac{1}{h_1} \frac{\partial \hat{\mathbf{q}}}{\partial x^1} \right\rangle + \text{c.c.}, \end{aligned}$$

where c.c. denotes the complex conjugate. The inner products $\langle \cdot, \cdot \rangle$ appearing above are defined as

$$\langle \psi, \phi \rangle = \int_{X_0}^{X_1} \int_{Z_0}^{Z_1} \int_0^{+\infty} \psi^H \phi h_1 dx^1 dx^2 dx^3, \quad (10)$$

for complex valued vectors ψ and ϕ . We can now define the problem as follows: find the control \dot{m}_w , states \mathbf{Q} , $\tilde{\mathbf{q}}$ and adjoint variables λ^* , χ^* , \mathbf{Q}^* , \mathbf{q}^* , and r^* such that \mathcal{L} is rendered stationary according to the first-order necessary condition for an extremal point. This is done by setting the first variation of \mathcal{L} with respect to the variables considered here to zero, while each of \mathcal{L} 's arguments are considered to be independent variables. This requirement comes from the fact that at an extremal point the first variation of \mathcal{L} with respect to each variable vanishes. We start by setting the first variation of \mathcal{L} with respect to each adjoint variable to zero, which gives the state equations (1), (3), and (4), and the constraint on the control effort, Eq. (8). We continue by setting the first variation of the state variables $\hat{\mathbf{q}}$, α , and \mathbf{Q} to zero. After a procedure which involves successive integrations by parts,⁸ this yields the adjoint equations

$$L_P^* \mathbf{q}^* = S_P^*, \quad (11)$$

$$\begin{aligned} \frac{\partial}{\partial x^1} \int_0^{+\infty} \mathbf{q}^{*H} \frac{\partial L_P}{\partial \alpha} \hat{\mathbf{q}} h_1 dx^3 \\ = \begin{cases} 0 & \forall x^1 \notin [X_{ms}, X_{me}], \\ -i|\Theta|^2 \int_0^{+\infty} \hat{\mathbf{q}}^H M \hat{\mathbf{q}} h_1 dx^3 & \forall x^1 \in [X_{ms}, X_{me}], \end{cases} \end{aligned} \quad (12)$$

$$L_B^* \mathbf{Q}^* = S_B^*, \quad (13)$$

where $\mathbf{q}^* = (\rho^*, u^*, v^*, w^*, \theta^*)^T$ and $\mathbf{Q}^* = (U^*, V^*, W^*, T^*)^T$. Equation (11) is the adjoint of the PSE (APSE) where u^* , v^* , w^* , and θ^* are subject to Dirichlet boundary conditions. The right-hand side S_P^* is due to the auxiliary condition of the PSE and the objective function. Equation (12) is a closure relation obtained by setting the first variation of \mathcal{L} with respect to the streamwise wave number α to zero. At each streamwise position, r^* is solved iteratively such that Eq. (12) is satisfied. Equation (13) is the adjoint of the BLE (ABLE) and the right-hand side S_B^* is the sensitivity of the PSE with respect to the mean flow. Both the APSE and ABLE are parabolic equations which are solved by backward integration in the streamwise direction. The above equations are found in Appendix A 2, and the complete derivations are found in Pralits *et al.*²³ and Pralits.²⁷ Finally, we set the first variation of \mathcal{L} with respect to \dot{m}_w to zero which gives the so-called optimality condition as

$$W_w^* + 2\chi^* \dot{m}_w = 0. \quad (14)$$

The left-hand side of the above expression is the gradient of the Lagrangian functional with respect to the mass flux at the wall. As shown in Eq. (9), χ^* is the adjoint variable used to enforce the control effort and can be solved iteratively in the optimization by substituting Eq. (14) into Eq. (8) as

$$\chi^* = \left(\frac{1}{4E_C} \int_{X_{cs}}^{X_{ce}} W_w^{*2} h_1 dx^1 \right)^{1/2}. \quad (15)$$

The complete optimality system contains Eqs. (1), (3), (4), and (11)–(15) which can be found in Appendix A.

A. Solution procedure

The procedure of solving the optimization problem derived in Sec. III is described here. We start by considering the case of minimizing a single disturbance, i.e., $K=1$ in Eq. (6).

The optimal distribution of the mass flow is found through an iterative procedure. During each iteration step, we perform successive calculations of boundary layer and stability equations from X_0 to X_1 ; and adjoint boundary layer and stability equations from X_1 to X_0 . Then, a new mass-flow distribution is computed using the gradient information given by solution of the adjoint equations. Here we use the L-BFGS-B optimization routine, see Zhu *et al.*,²⁸ Byrd *et al.*²⁹ The calculations are repeated until the relative change in the objective function is less than a prescribed value.

If $K>1$ in Eq. (6) then instead of solving both state and adjoint equations K times, we can utilize the fact that the ABLE are linear equations. In this case the optimality condition is evaluated as follows: the BLE is solved once; the PSE and APSE are solved K times; the forcing of the ABLE, S_B^* , is calculated as

$$S_B^* = \sum_{k=1}^K S_{B_k}^*.$$

Finally, the optimality condition is evaluated from a single calculation of the ABLE.

The results presented here are obtained by numerically integrating the discretized state and adjoint equations. The x^1 derivatives are approximated by a first- or second-order accurate backward Euler scheme. The x^3 derivatives of the PSE and APSE are approximated by a fourth-order accurate compact finite-difference scheme and a second-order accurate finite-difference scheme for the BLE and ABLE. The convergence criteria is $(J^{k+1} - J^k)/J^k < 10^{-4}$, where k denotes the iteration number in the optimization procedure. Further, in all calculations the initial guess on the suction profile, \dot{m}_w^{in} , has been varied to make sure that the optimal solution does not depend on the initial state.

B. Case studied

The flow studied here is the boundary layer on the upper side of a wing designed for commercial aircraft. The flow conditions are characterized by a free stream Mach number $M_\infty=0.8$, temperature $T_\infty=230$ K, Reynolds number $Re_\infty=3.04 \times 10^7$ and leading edge sweep angle $\phi_{le}=30.2^\circ$. The control domain, $\Gamma_c=[X_{cs}, X_{ce}]$, available for mounting the

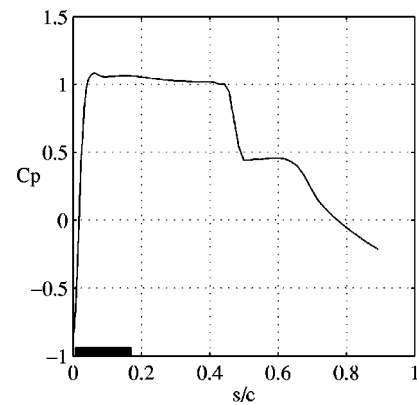


FIG. 2. The pressure distribution, C_p , as a function of the arc-length normal to the leading edge, s/c . The black box shows the available control domain, Γ_c .

suction system has been specified by the manufacturer. The control domain is limited in the upstream direction, $0 < s/c < 0.006$, by a suction strip used to control the stagnation line and in the downstream direction by the front spar ($s/c=0.17$). Here s is the arc-length normal to the leading edge measured from the stagnation point and c is the chord length. The suction strip at the stagnation line is case specific and will be held unchanged. However, this does not create any difficulties in the optimization procedure. In Fig. 2 the pressure coefficient C_p is plotted as a function of s/c . The available control domain $0.006 \leq s/c \leq 0.17$ is also indicated in this figure as a black box.

Parameters for the disturbances analyzed here are given in Table I. At the initial streamwise position ($s/c=0.0075$), the flow has a strong favorable pressure gradient and the mean flow velocity component perpendicular to the outer streamline has an inflection point. There, waves with the wave number vector \mathbf{k} approximately perpendicular to the outer streamline have positive growth rate. These are the so-called cross-flow (CF) waves. Further downstream ($s/c=0.05$) where the pressure gradient is weaker and adverse, Tollmien–Schlichting (TS) waves are amplified. The angles between the wave number vectors of the TS waves analyzed here and the outer streamline are 0–60 degrees. In Fig. 3 the envelope of envelopes (EoE) of the N_E -factor curves are plotted for the CF and TS disturbances given in Table I and for zero suction rate.

The control effort which is quantified by Eq. (8) depends on the specific suction system chosen, i.e., compressors and tubing. We have therefore chosen a number of different mag-

TABLE I. Initial position ($s/c=X_0$), dimensional frequency (f^*), dimensional spanwise wave number (β^*) and type of disturbances analyzed (CF=cross-flow wave, TS=Tollmien–Schlichting wave). Δf^* and $\Delta \beta^*$ denote respective dimensional step-length.

X_0	f^*	Δf^*	β^*	$\Delta \beta^*$	Type
0.0075	[1000, 8500]	500	[1000, 6000]	500	CF
0.0075	0	0	[500, 6500]	500	CF
0.05	[2250, 9500]	250	0	0	TS
0.05	[2250, 7000]	250	[25, 225]	50	TS

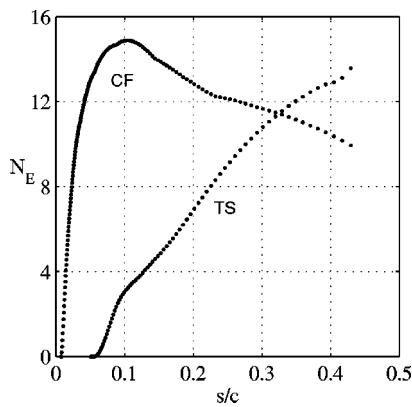


FIG. 3. Envelope of envelopes of N_E -factor curves for the two disturbance types given in Table I for the case of zero suction.

nitudes of E_C to examine the dependency of the achieved stabilization on the amplitude of the control energy. Here we introduce a new parameter $Q_C = E_C Re_\infty$. In our calculations the values of Q_C are chosen so that a noticeable control effect is achieved and to avoid the magnitude of mean wall-normal velocity (at the wall) W_w exceeding $O(Re^{-1})$. This was checked after each calculation.

C. Results

Results are shown here for minimization of the disturbance kinetic energy, Eq. (7), in which ξ has been chosen depending on the desired objective function. When $\xi=1$, the measure is given as the sum of the kinetic energy of K disturbances. Before the optimization is performed, it has to be decided if one or several disturbances should be included. One of the conclusions from Pralits *et al.*⁸ and Airiau *et al.*⁹ was that the optimal suction distribution for a given disturbance will also have a damping effect on other disturbances of the same type. The reason for including more than one disturbance in the measure⁸ is that in some cases it is not clear which type of disturbance will cause laminar-turbulent transition first. Another reason is that if different types of disturbances are present in the flow, then the mean-flow

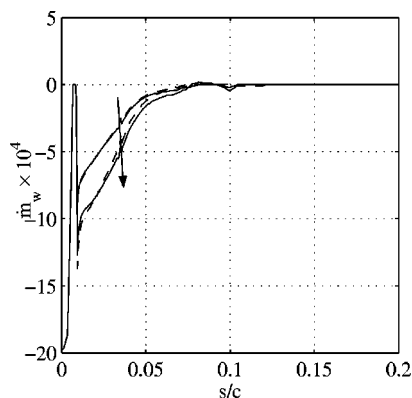


FIG. 4. Optimal suction distributions, m_w , minimizing the disturbance kinetic energy of a CF wave ($f^* = 5500 \text{ s}^{-1}$, $\beta^* = 2500 \text{ m}^{-1}$) measured as E_Ω (dashed), E_f (solid). $Q_C = 0.35$ and 0.58 , and the arrow marks increasing Q_C .

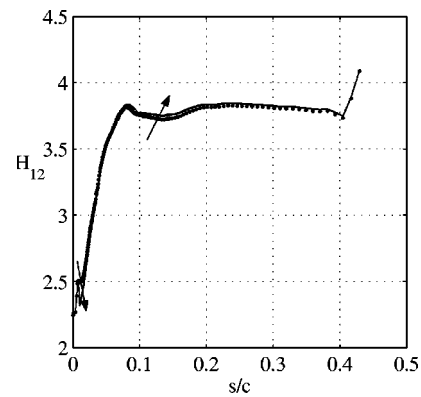


FIG. 5. Shape factor, H_{12} , given zero (dotted) and optimal suction distribution from Fig. 4 minimizing the disturbance kinetic energy of a CF wave ($f^* = 5500 \text{ s}^{-1}$, $\beta^* = 2500 \text{ m}^{-1}$) measured as E_Ω (dashed), E_f (solid). $Q_C = 0, 0.35$, and 0.58 , and the arrow marks increasing Q_C .

modification that minimizes some measure of one type of disturbance may amplify rather than damp disturbances of another type. One should keep in mind that the larger number of disturbances considered, the more costly the optimization procedure will be.

As a first investigation, a comparison is made between minimizing the kinetic energy of a single disturbance integrated in a streamwise domain ($\xi=1$), with the case of minimizing the same disturbance at a final streamwise position ($\xi=0$).

Equation (6) is integrated between X_0 and the end of the control domain which means that the aim is to delay transition at least up to this position. X_f in Eq. (5) is chosen as the position where the maximum disturbance kinetic energy is found over all disturbances in Table I, here $X_f = 0.105$. The corresponding disturbance, which also has the largest E_Ω over all disturbances in Table I, is chosen as the one to minimize in both cases. This disturbance is a CF wave with dimensional frequency and spanwise wave number of 5500 s^{-1} and 2500 m^{-1} , respectively. The calculations are performed for $Q_C = 0.25, 0.35, 0.45$, and 0.58 .

The optimal suction distributions given by the two

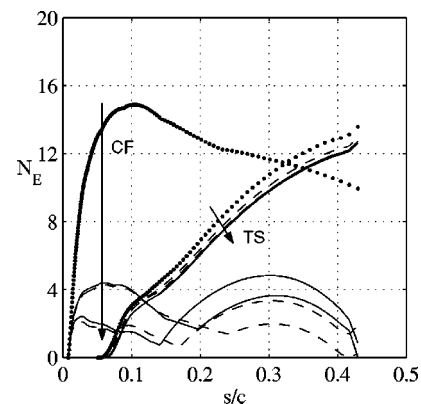


FIG. 6. Envelope of envelopes of N_E -factor curves for the disturbances given in Table I given zero (dotted) and optimal suction distribution from Fig. 4 minimizing the disturbance kinetic energy of a CF wave ($f^* = 5500 \text{ s}^{-1}$, $\beta^* = 2500 \text{ m}^{-1}$) measured as E_Ω (dashed), E_f (solid). $Q_C = 0, 0.35$ and 0.58 , and the arrows mark increasing Q_C .

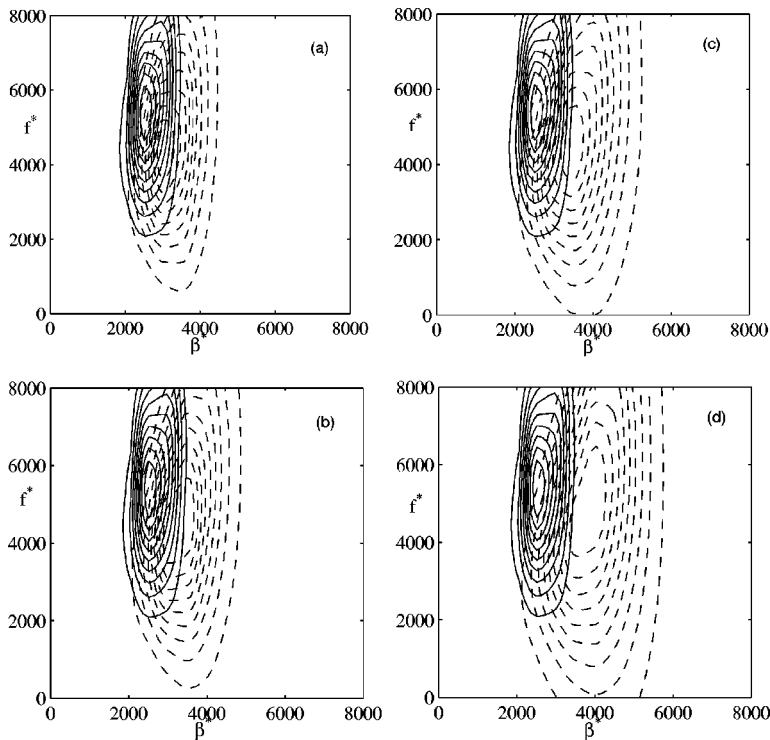


FIG. 7. Contours of E_{Ω} for CF waves comparing zero (solid) and optimal suction distribution (dashed) minimizing the disturbance kinetic energy of a CF wave ($f^* = 5500 \text{ s}^{-1}$, $\beta^* = 2500 \text{ m}^{-1}$). Both cases are normalized with their respective maximum value and the contour spacing=0.1. The control effort Q_C and the ratio between the maximum values are, respectively, (a) 0.25, 1.4×10^{-8} ; (b) 0.35, 6.7×10^{-10} ; (c) 0.45, 6.4×10^{-11} ; (d) 0.58, 5.5×10^{-12} .

different objective functions can be seen in Fig. 4. Here, results are only shown for two different values of the control energy to make the plot more clear. The arrow indicates the direction of increasing Q_C and the uppermost streamwise suction distribution is the fixed stagnation line control. It is interesting to note the similarity between the results when comparing the two objective functions as opposed to a similar comparison for control of TS waves reported by

Airiau *et al.*⁹ The reason for this may be that the growth and decay of CF waves in the case analyzed here occurs over a short streamwise interval, and as a consequence the growth measured by E_{Ω} approach that for E_f . In all cases, the optimal control acts primarily in the region where a strong favorable pressure gradient exists and then decays further downstream. As the control effort is increased, the additional control energy is concentrated to the beginning of the control

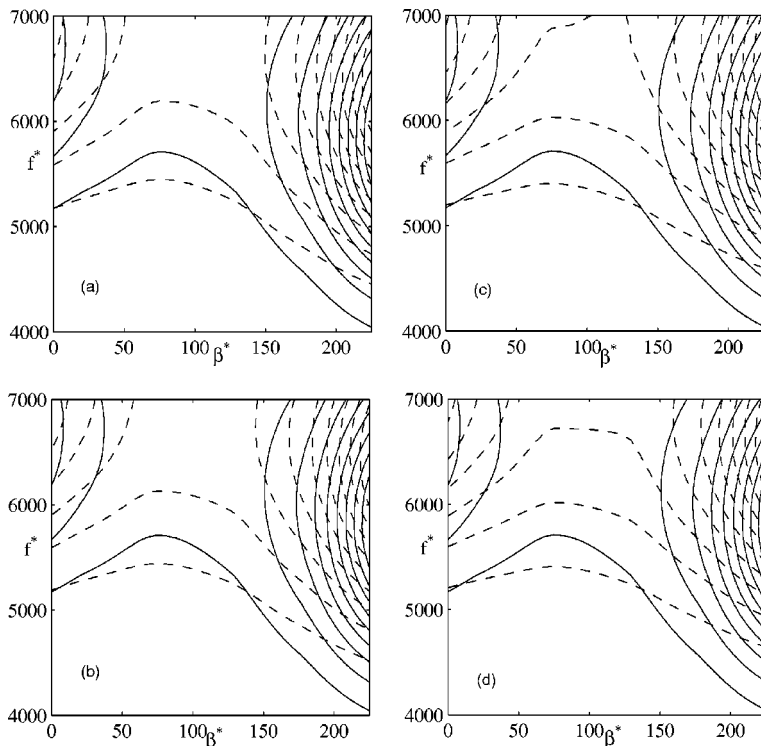


FIG. 8. Contours of E_{Ω} for TS waves comparing zero (solid) and optimal suction distribution (dashed) minimizing the disturbance kinetic energy of a CF wave ($f^* = 5500 \text{ s}^{-1}$, $\beta^* = 2500 \text{ m}^{-1}$). Both cases are normalized with their respective maximum value and the contour spacing=0.1. The control effort Q_C and the ratio between the maximum values are, respectively, (a) 0.25, 0.21; (b) 0.35, 0.16; (c) 0.45, 0.1; (d) 0.58, 0.092.

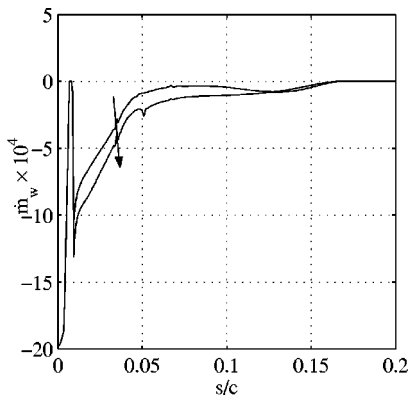


FIG. 9. Optimal suction distributions, \dot{m}_w , minimizing the disturbance kinetic energy E_Ω of a CF ($f_1^* = 5500 \text{ s}^{-1}$, $\beta_1^* = 2500 \text{ m}^{-1}$) and TS wave ($f_2^* = 5750 \text{ s}^{-1}$, $\beta_2^* = 225 \text{ m}^{-1}$). $Q_C = 0.35$ and 0.58 , and the arrow marks increasing Q_C .

domain. The effect of the control on the shape factor is however small, which can be seen in Fig. 5.

The magnitudes of the suction distributions presented in this paper are all within the range of validity for the boundary layer equations, i.e., of order $O(\text{Re}^{-1})$. This was investigated by Airiau *et al.*,⁹ where suction distributions with magnitudes within the limits experienced locally rapid streamwise variations. They compared solutions from the Navier–Stokes equations with those using the boundary layer equations. They found that the pressure gradient from the Navier–Stokes solution varies rapidly close to the suction peak but relaxes very rapidly downstream where it becomes small, in accordance with the parabolic assumption of the boundary layer equations. They further showed that shape factors from the boundary layer and Navier–Stokes solutions agree well and conclude that there is a weak dependence of the shape factor on the mean pressure gradient and that the solutions of the boundary-layer equations are valid.

In Fig. 6, the EoE of the N_E -factor curves of CF and TS waves are plotted for the cases of zero and optimal suction distributions shown in Fig. 4. In the control domain, the CF waves are more damped as Q_C is increased. However, downstream of the control region the CF waves are increasingly amplified as Q_C is increased. As expected the TS waves are less affected by the controls since we know that the control acts upstream of the region where the TS waves are amplified.

In the results shown here, the optimal suction distributions are based on minimizing a single disturbance only. The damping effect of such a control on other disturbances of the same type can be seen from EoE curves given in Fig. 6. In

Figs. 7 and 8, this has been emphasized by plotting contours of E_Ω for CF and TS waves in the (f^*, β^*) -plane comparing zero and optimal suction distributions for all values of Q_C . In all cases the kinetic energy of all disturbances has been reduced. It is clear from the ratio between the maximum value of E_Ω for the zero and optimal control, that the CF waves are mostly affected. This is true for all values of Q_C studied here.

From these results, as discussed in Pralits *et al.*⁸ and Airiau *et al.*,⁹ one can conclude that minimizing the disturbance kinetic energy of one disturbance (in this case CF waves) does have a damping effect on other disturbances of the same type. To confirm this, computations were also performed in which the TS wave with the largest total disturbance kinetic energy was controlled. The suction distribution from these calculations had a damping effect on all other TS waves. These results are not shown here.

The absence of control in the region where the TS waves are amplified can be overcome by adding a disturbance of TS type in the objective function when $\xi = 1$. Therefore, as a next step both the CF and TS wave with the largest E_Ω over all respective disturbances in Table I are considered. The dimensional frequency and spanwise wave number for the TS wave are 5750 s^{-1} and 225 m^{-1} , respectively, and the calculations are performed with the same values of Q_C used for control of a single CF wave.

In Table II the ratio between the maximum values of E_Ω for CF waves using optimal and zero suction are given. Here, we compare the case of optimal suction based on minimizing a CF wave with the case of minimizing the sum of a CF and a TS wave. It is seen that the change of the ratio is small between the cases, even when Q_C is increased. In Table III the same comparison is done for the ratio of the maximum values of E_Ω for TS waves. Here, it is clear that the ratio has decreased when both CF and TS disturbances are considered. As the same amount of control effort is used, this means that Q_C is redistributed in the streamwise direction to control the TS wave. The corresponding optimal suction distributions are plotted in Fig. 9 for the cases when $E_C = 0.35$ and 0.58 . The suction distributions in the upstream part of the control domain are similar to the ones in Fig. 4, but the magnitudes are smaller. Further downstream, the suction distribution is rather constant before it goes to zero at the end of the control domain. The latter is similar to what is shown in Pralits *et al.*⁸ for control of two-dimensional TS waves in two-dimensional boundary layer flows when a small control effort is used. The effect of the control on the shape factor is plotted in Fig. 10. Compared to the results given in Fig. 5, a larger decrease of H_{12} occurs in the downstream portion of the control domain. The corresponding thinning of the

TABLE II. Ratio between maximum values of E_Ω for CF waves when zero and optimal suction distribution minimizing the disturbance kinetic energy is applied. The ratio is calculated when Eq. (6) includes CF and CF+TS for different values of Q_C .

Disturbance	$Q_C = 0.25$	$Q_C = 0.35$	$Q_C = 0.45$	$Q_C = 0.58$
CF	1.4×10^{-8}	6.7×10^{-10}	6.4×10^{-11}	5.5×10^{-12}
CF+TS	2.2×10^{-8}	1.4×10^{-9}	5.7×10^{-11}	1.1×10^{-11}

TABLE III. Ratio between maximum values of E_Ω for TS waves when zero and optimal suction distribution minimizing the disturbance kinetic energy is applied. The ratio is calculated when Eq. (6) includes CF and CF+TS for different values of Q_C .

Disturbance	$Q_C=0.25$	$Q_C=0.35$	$Q_C=0.45$	$Q_C=0.58$
CF	2.1×10^{-1}	1.6×10^{-1}	1.0×10^{-1}	9.2×10^{-2}
CF+TS	6.1×10^{-3}	8.6×10^{-3}	1.1×10^{-3}	6.6×10^{-3}

boundary layer is favorable in terms of damping the TS waves. The EoE of the N_E -factor curves are plotted in Fig. 11. Here, the CF waves are less damped compared to the previous case, see Fig. 6. However, the TS waves are now more damped.

It is of interest to know if a larger reduction of the disturbance kinetic energy can be obtained for a given control effort if additional modes, apart from the two discussed here, are included in the calculations. Such a parameter study has been performed and the results show that the additional decrease in disturbance kinetic energy is small when more modes are included. The reason is that the control mainly acts on the modes with the largest energy. Since the control affects all other disturbances (shown here), it will continue to act on the mode with the initially largest energy even if additional modes are included.

IV. SIMPLIFIED APPROACH

In design of suction distributions for the purpose of delaying laminar-turbulent transition, it is important that the procedure is not computationally expensive. The same argument can be made when designing on-line control systems, where fast feedback is needed. For this purpose, an alternative approach was analyzed in Airiau *et al.*⁹ for the control of TS waves in incompressible flat-plate boundary layers. In their study the optimal suction distribution is computed by minimizing the streamwise integral of the shape factor. This means that only the boundary layer and corresponding adjoint equations are involved in the optimization process which is computationally more efficient. However, the effect of the optimal suction distribution on the disturbance growth is analyzed afterwards. This choice of objective function is

based on the knowledge that any thinning of the boundary layer has a stabilizing effect on the boundary layer. Successful results are shown for control of TS waves. The positive features of this approach motivates an investigation here.

A. Optimality system

The objective function is now given as

$$\mathcal{J}_0 = \int_{x_{ms}}^{x_{me}} H_{12} h_1 dx^1,$$

where

$$H_{12} = \frac{\delta_1}{\delta_2} = \frac{\int_0^{+\infty} \left(1 - \frac{\rho U_{SL}}{\rho_e Q_e}\right) dx^3}{\int_0^{+\infty} \frac{\rho U_{SL}}{\rho_e Q_e} \left(1 - \frac{U_{SL}}{Q_e}\right) dx^3}. \quad (16)$$

Both the displacement δ_1 and momentum thickness δ_2 are based on the velocity component $U_{SL} = U \cos(\phi) + V \sin(\phi)$ which is in the direction of the outer streamline. Here $\phi = \tan^{-1}(V_e/U_e)$ and $Q_e = (U_e^2 + V_e^2)^{1/2}$. Now, only one state equation is considered and the problem consists of finding the control \dot{m}_w , and corresponding state \mathbf{Q} which minimizes \mathcal{J}_0 given the constraints shown in Eqs. (1) and (8). The technique using Lagrange multipliers is also used here to enforce the constraints. The adjoint variables \mathbf{Q}^* , λ^* , χ^* are introduced and the new Lagrangian functional is given as

$$\mathcal{L} = \mathcal{J}_0 - \mathcal{J}_1, \quad (17)$$

where \mathcal{J}_1 is now written

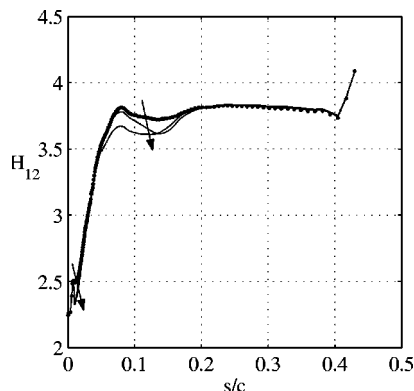


FIG. 10. Shape factor, H_{12} , given zero (dotted) and optimal suction distribution (solid) from Fig. 9 minimizing the disturbance kinetic energy E_Ω of a CF ($f_1^* = 5500 \text{ s}^{-1}$, $\beta_1^* = 2500 \text{ m}^{-1}$) and TS wave ($f_2^* = 5750 \text{ s}^{-1}$, $\beta_2^* = 225 \text{ m}^{-1}$). $Q_C = 0, 0.35$ and 0.58 , and the arrow marks increasing Q_C .

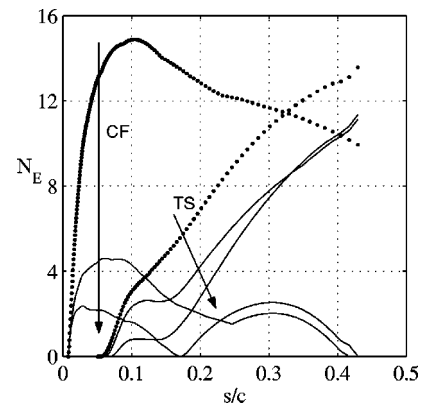


FIG. 11. Envelope of envelopes of N_E -factor curves for the disturbances given in Table I given zero (dotted) and optimal suction distribution from Fig. 9 minimizing the disturbance kinetic energy E_Ω of a CF ($f_1^* = 5500 \text{ s}^{-1}$, $\beta_1^* = 2500 \text{ m}^{-1}$) and TS wave ($f_2^* = 5750 \text{ s}^{-1}$, $\beta_2^* = 225 \text{ m}^{-1}$). $Q_C = 0, 0.35$, and 0.58 and the arrows mark increasing Q_C .

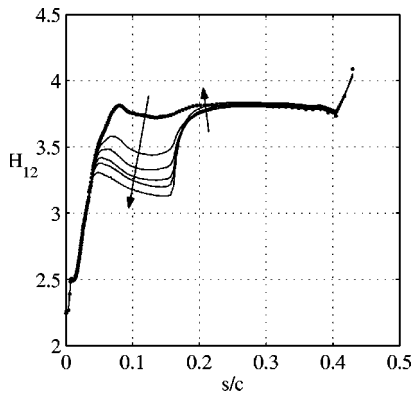


FIG. 12. Shape factor, H_{12} for zero (dotted) and optimal suction distributions (solid) minimizing the shape factor. $Q_C=0, 0.1, 0.3, 0.58, 0.81,$ and 1.43 and the arrows mark increasing Q_C .

$$\mathcal{J}_1 = \langle \mathbf{Q}^*, L_B \mathbf{Q} \rangle + \int_{X_{cs}}^{X_{ce}} \lambda^* [\dot{m}(x^1, 0) - \dot{m}_w] h_1 dx^1 + \chi^* \left(E_C - \int_{X_{cs}}^{X_{ce}} \dot{m}_w^2 h_1 dx^1 \right).$$

The derivation is performed as previously described which yields an optimality system which contains the BLE, Eq. (1), corresponding adjoint equation and optimality condition. Compared to the previously derived ABLE, differences occur in the boundary conditions and forcing term S_B^* . These differences are due to the objective function, Eq. (16). Details of the optimality system can be seen in Appendix B.

B. Results

Results are shown here on minimizing the shape factor. First we consider control in the whole available domain Γ_c , and the objective function is integrated in the same streamwise region used for Eq. (6) in Sec. III C. The control efforts in these calculations are $Q_C=0.1, 0.3, 0.58, 0.81,$ and 1.43 . In Fig. 12 the shape factors for these cases are compared to that of the uncontrolled case. As the control effort is increased, the shape factor is decreased within the major part of the control domain. Downstream of the control domain a small increase of the shape factor is observed. The corre-

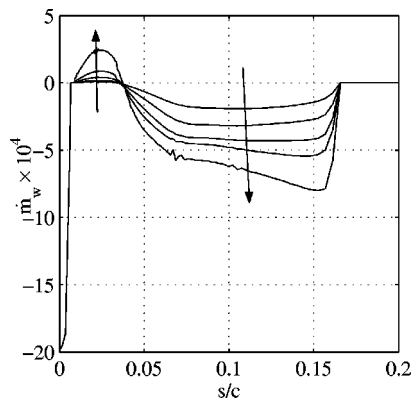


FIG. 13. Optimal suction distributions, \dot{m}_w , minimizing the shape factor, H_{12} . $Q_C=0.1, 0.3, 0.58, 0.81, 1.43$ and the arrows mark increasing Q_C .

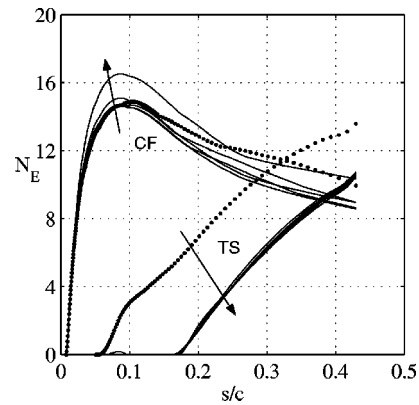


FIG. 14. Envelope of envelopes of N_E -factor curves for the two disturbance types given in Table I given zero (dotted) and optimal suction distribution minimizing (solid) the shape factor. $Q_C=0, 0.1, 0.3, 0.58, 0.81, 1.43$ and the arrows mark increasing Q_C .

sponding suction profiles are plotted in Fig. 13. Note that the uppermost streamwise suction distribution is due to the stagnation line control which is taken to be fixed. In all cases, the optimal control is divided roughly at $s/c=0.04$ into blowing upstream and suction downstream, and the magnitude of the control is increased in both regions as Q_C is increased. At this position the flow goes from a strongly accelerating one to a weakly decelerating one.

Compared to Fig. 3, one can see that the region of blowing is where the CF waves are amplified and the region of suction is where the TS waves are amplified. In Fig. 14 the EoE of the N_E -factor curves for CF and TS waves are plotted for zero and optimal suction distributions ($Q_C=0,0.1,0.3,0.58,0.81,1.43$). When control is applied, the TS waves are completely stabilized in the control domain and are then amplified downstream, except for $Q_C=0.1$. The CF waves are instead amplified in the region where blowing occurs and this becomes more pronounced as Q_C is increased. For the airfoil analyzed here, this means that applying an optimal control based on minimizing the streamwise integral of the shape factor will not delay but rather precipitate laminar-turbulent transition.

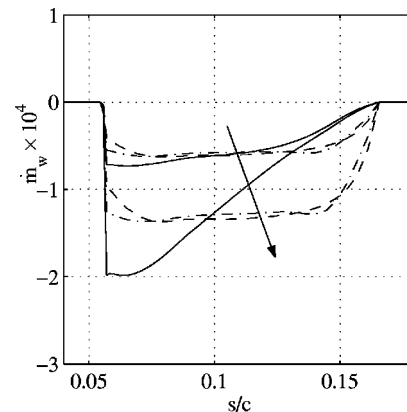


FIG. 15. Comparison of optimal suction distributions for the cases of minimizing the disturbance kinetic energy of a TS wave measured as E_Ω (solid), E_f (dashed-dotted), and the case of minimizing the shape factor (dashed). $Q_C=0.01, 0.05,$ and the arrow indicates increasing Q_C .

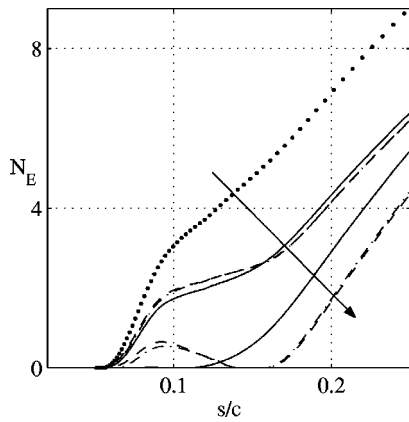


FIG. 16. Comparison of envelope of envelopes of N_E -factor curves for the cases of minimizing the disturbance kinetic energy of a TS wave measured as E_O (solid), E_f (dashed-dotted), the case of minimizing the shape factor (dashed), and zero control (dotted). $Q_C=0, 0.01, 0.05$, and the arrow indicates increasing Q_C .

In the results shown so far, the most efficient way to control CF waves is a suction distribution based on minimizing the most amplified CF wave. The TS waves, on the other hand, have so far shown to be more efficiently controlled using the suction distribution based on minimizing the shape factor. In order to further investigate the control of TS waves, the case of minimizing the shape factor is compared with the cases of minimizing the integrated disturbance kinetic energy of a TS wave and its value at a given streamwise position X_f . The latter two objective functions are obtained by setting ξ equal to one and zero, respectively, in Eq. (7). In this comparison, a smaller control domain, $\Gamma_C=[0.05,0.17]$, is used, as the TS waves are amplified downstream of the region with negative pressure gradient. The disturbances are measured at $X_f=X_{ce}$ and in the control domain for ξ equals zero and one respectively. For the comparison, a noticeable reduction in the disturbance growth is obtained choosing the control effort as $Q_C=0.01$ and 0.05 . The corresponding suction distributions can be seen in Fig. 15. For the cases of minimizing the shape factor, and the disturbance kinetic energy at X_f evenly distributed suction distributions are obtained for both values of Q_C . The suction distributions based on minimizing the total disturbance kinetic energy, on the other hand, concentrates the control effort close to the lower branch of the neutral curve. The corresponding EoE of the N_E -factor curves for TS waves are shown in Fig. 16 and are compared with the uncontrolled case. In all cases when control is applied a reduction of the disturbance growth is obtained. When the lower value of the control effort is used, the difference between the three approaches is small, see also Fig. 15. As the control effort is increased, the suction distribution based on minimizing the E_O completely stabilizes the disturbances upstream of $s/c \approx 0.12$. The other two approaches, due to the evenly distributed suction, produce a continuous thinning of the boundary layer and consequently larger damping of disturbances downstream.

V. CONTROL USING PRESSURE CHAMBERS

The most common approach for computing optimal suction distributions is to use the wall mass flux as the control variable.^{6,8,9} In a realistic setting, such as an experiment or suction systems used on wings, the suction velocity is a function of the surface porosity, hole geometry and the pressure difference between the pressure distribution on the surface and static pressure in a number of discrete chambers.^{1,14-17} The aim here is to derive the optimal control problem of Sec. III using the static pressures of a number of discrete chambers, with fixed size and position, as control variables. We will then compare the results with the previously computed continuous suction distribution to assess the feasibility of the latter approach.

If a porous surface is used, then at least for flows with low free-stream velocity, the relation between the pressure difference and the suction velocity is linear, in accordance with Darcy's law. The relation between the pressure difference and suction velocity used here is taken from Bieler and Preist.¹⁷ It is based on measurements carried out in the framework of the ELFIN (European Laminar Flow INvestigation) program. In dimensionless form this formula is given as

$$\Delta P_j = \frac{C_1}{\rho_w} \dot{m}_w^2 + C_2 \frac{\mu_w}{\rho_w} \dot{m}_w \quad \forall x^1 \in [X_{cs_j}, X_{ce_j}],$$

$$j = 1, \dots, K, \quad (18)$$

where $\Delta P_j = P_e - P_{c_j}$, in which P_e is the pressure distribution on the wing and P_{c_j} is the static pressure in chamber j . The first term on the right-hand side of Eq. (18) is due to the dynamic pressure loss, and the second term is the pressure loss due to skin friction. The coefficients C_1 and C_2 together with a brief description of Eq. (18) are given in Appendix C. The choice of static pressure in the chambers is not without restrictions. The Mach number of the flow through the holes of the porous plate should be limited. If ΔP_j is too small then blowing instead of suction might occur. Disturbances might be introduced as an effect of strong suction through discrete holes, which can accelerate instead of delay laminar-turbulent transition.^{14,15} These restrictions are related to the design of the perforated plate and therefore not considered as constraints in the theory presented here.

A. Optimality system

Here a concise description of the derivation of the optimality system including pressure chambers is given for the case of minimizing the disturbance kinetic energy. The optimal control problem is now defined as: find controls P_{c_j} , and states \mathbf{Q} and $\tilde{\mathbf{q}}$ which minimize the objective function \mathcal{J}_0 given by Eq. (7) with the constraints given by Eqs. (1), (3), (4), and (8). The Lagrange multiplier technique is also used here to enforce the constraints. The adjoint variables \mathbf{Q}^* , \mathbf{q}^* , r^* , χ^* , and λ_j^* where $j = 1, \dots, K$, are introduced and the new Lagrangian functional is given as

$$\mathcal{L} = \mathcal{J}_0 - \mathcal{J}_1, \quad (19)$$

where

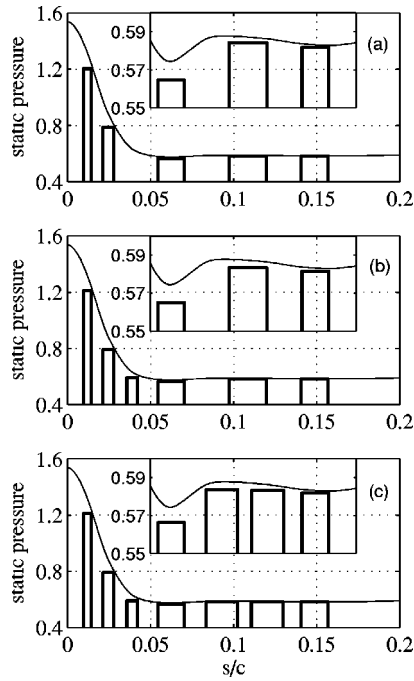


FIG. 17. Pressure distribution on the wing (thin lines) and optimal static pressure in the chambers (thick lines) for the cases of (a) 5, (b) 6, and (c) 7 pressure chambers minimizing the disturbance kinetic energy E_Ω of a CF ($f_2^* = 5500 \text{ s}^{-1}$, $\beta_1^* = 2500 \text{ m}^{-1}$) and TS wave ($f_2^* = 5750 \text{ s}^{-1}$, $\beta_2^* = 225 \text{ m}^{-1}$) when $Q_C = 0.35$.

$$\begin{aligned} \mathcal{J}_1 = & \langle \mathbf{Q}^*, L_B \mathbf{Q} \rangle + \sum_{j=1}^K \int_{X_{cs_j}}^{X_{ce_j}} \lambda_j^* [\dot{m}(x^1, 0) - \dot{m}_w] h_1 dx^1 \\ & + \chi^* \left(E_C - \sum_{j=1}^K \int_{X_{cs_j}}^{X_{ce_j}} \dot{m}_w^2 h_1 dx^1 \right) + \langle \mathbf{q}^*, L_P \hat{\mathbf{q}} \rangle \\ & + \left\langle r^* \hat{\mathbf{q}}, \frac{1}{h_1} \frac{\partial \hat{\mathbf{q}}}{\partial x^1} \right\rangle + \text{c.c.} \end{aligned}$$

Compared to the previously described Lagrangian functionals, the wall boundary condition has now been divided into K discrete domains, and the mass flux at the wall is given by Eq. (18). No additional difficulties appear in the derivation compared to the one in Sec. III. The optimality condition is now obtained by setting the functional derivative with respect to the static pressure of each chamber to zero. The resulting optimality system can be seen in detail in Appendix C.

B. Results

Here results are given for the case of minimizing the disturbance kinetic energy using pressure chambers. The parameters in Eq. (18) which specify the porous surface are taken from Bieler and Preist.¹⁷ The plate thickness L and hole diameter at the surface d are 0.9 mm and 0.046 mm, respectively. The porosity $\pi/(4\epsilon^2)$ is calculated given a hole pitch to diameter ratio $\epsilon = 13.8$. The coefficients of inertial and viscous pressure loss are $A = 1.6$ and $B = 0.092$, respectively.

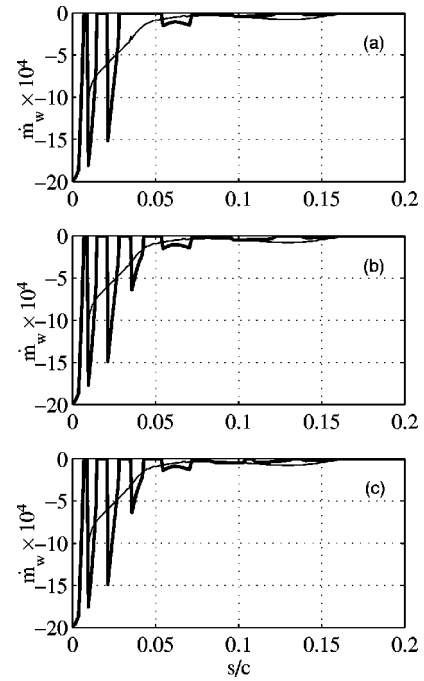


FIG. 18. Suction distributions (thick lines) corresponding to the optimal pressure drop for the cases of (a) 5, (b) 6, and (c) 7 pressure chambers in Fig. 17. A comparison is done with the optimal suction distribution (thin lines) from Fig. 9 when $Q_C = 0.35$.

Before the calculations are performed, the size, position and number of pressure chambers must be set. The different sizes are chosen such that the chambers are smaller where the pressure gradient of the wing is large and vice versa. This is done to avoid large pressure drops which result in large suction peaks. The whole control domain $\Gamma_c = [X_{cs}, X_{ce}]$ is used such that the pressure chamber closest to the leading edge starts at $X_{cs_1} = X_{cs}$ and the last pressure chamber ends at $X_{ce_K} = X_{ce}$.

The results in Sec. IV B show that minimizing the shape factor does not always give an optimal suction distribution which reduces the disturbance growth. Further, it is seen in Sec. III C that both CF and TS type disturbances should be included in the calculations when the disturbance kinetic energy is minimized. Therefore, we choose to minimize the total disturbance kinetic energy, $\xi = 1$ in Eq. (7), including both the CF and TS waves given in Sec. III C. The control effort $Q_C = 0.35$ and the calculations are done for the cases of 5, 6, and 7 pressure chambers.

Results of the optimal static pressures P_{c_j} of each case are plotted (thick lines) in Fig. 17. The pressure distribution on the wing P_e is also plotted (thin lines) for comparison. The region $s/c = [0.05, 0.175]$ has been magnified to enhance the details. As shown, the pressure difference $\Delta P_j = P_e - P_{c_j}$ is larger close to the leading edge and decreases downstream.

The suction distributions corresponding to the optimal static pressures in Fig. 17 are plotted in Fig. 18. Note that the uppermost streamwise suction distribution in each case is due to the stagnation line control and is taken to be fixed. In each case the suction distribution downstream of $s/c = 0.05$

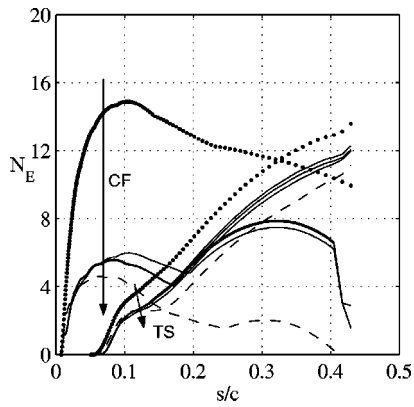


FIG. 19. Envelope of envelopes (EoE) of N_E -factor curves for the disturbances given in Table I for the cases of zero control (dotted) and the optimal pressure chambers in Fig. 17 (solid). The arrows mark increasing number of pressure chambers. A comparison is done with the EoE of N_E -factor curves (dashed) from Fig. 11 with $Q_c=0.35$.

is rather constant. Upstream of this streamwise position the suction distributions have more of a sawtooth shape. The latter is an effect of the strong pressure gradient in this region.

For each case in Fig. 18, a comparison is made with the optimal suction distribution from Fig. 9 (thin lines) for the case when $Q_c=0.35$. As the same control effort is used in these calculations, it is interesting to compare the optimal suction distribution in a continuous control domain with the cases using pressure chambers. It is seen that the magnitude of both the suction distribution from Fig. 9 and the suction distributions using pressure chambers is rather constant downstream of $s/c=0.05$ and increases upstream of this position. Further, the distribution using pressure chambers approaches the continuous one when the number of chambers is increased. This is most evident downstream of $s/c=0.05$.

The effect on the disturbance growth using the optimal pressure differences for the cases of 5, 6, and 7 pressure chambers is shown in Fig. 19. Here the EoE of the N_E -factor curves for CF and TS waves are plotted for zero and optimal pressure differences of all cases (solid lines). The arrows mark the direction of increasing number of pressure chambers. A decrease in the growth of both CF and TS waves is obtained for all optimal pressure differences calculated here compared to the case of zero suction. The CF waves are more damped in the control domain when the number of pressure chambers is increased. However, the difference between the cases of having 6 and 7 pressure chambers is small as the additional chamber is placed where the CF waves begin to decay. The results for the TS waves show that upstream of $s/c=0.1$, the EoE curves increase in magnitude as the number of pressure chambers increases. Downstream of this position EoE curves decrease in magnitude. A comparison is made with the EoE of the N_E -factor curves in Fig. 11 which are calculated using the suction distribution from Fig. 9 with $Q_c=0.35$ (dashed lines). It is seen that as the number of pressure chambers are increased, the results within the control domain using pressure chambers approach those us-

ing a suction distribution in a continuous control domain. This is true for the results of both the CF and TS waves.

VI. DISCUSSION AND CONCLUSIONS

A method to control convectively unstable disturbances in boundary layers on infinite swept wings for compressible fluids has been derived and analyzed. The method has been developed in the framework of optimal control theory. The mean of disturbance control is a modification of the mean flow by the mass flow through a porous surface. The optimization problem is derived using Lagrange multipliers from which optimality systems are obtained containing the adjoint of the parabolized stability equations (APSE) and the adjoint of the boundary layer equations (ABLE).

Two different control variables are considered. The first control variable is the mass flow at the wall. Here, it is assumed that given a certain control domain, the suction distribution is not constrained by how it will be implemented on the wing and thus has the optimal distribution with respect to a certain objective function. The second control variable is the static pressure in a number of pressure chambers. Here, the suction velocity is a function of the surface porosity, hole geometry and the pressure difference between the pressure distribution on the wing and the internal static pressure of the pressure chambers. In this case, the internal static pressure of each box is optimized. In both cases, the control effort has not been regularized, but instead enforced as a constraint.

Different measures of the state (objective functions) have been analyzed. The first objective function is a measure of the disturbance kinetic energy. A comparison has been made between minimizing the kinetic energy of a single disturbance at a fixed streamwise position, and minimizing the streamwise integral of the kinetic energy of an arbitrary number of disturbances. For control of a single CF wave, the difference between the two objective functions is small. The advantage of the latter is that more than one disturbance can be included in the measure. On the wing studied here, both cross flow and TS waves are amplified on the upstream part. Results show that both disturbance types need to be accounted for in the objective function in order for the control to decrease their growth. Further, it is sufficient to account for one of each disturbance type in order to control all other disturbances of the same type.

The second measure of the state used here is the streamwise integral of the shape factor, H_{12} . Airiau *et al.*⁹ showed that this quantity is successful for control of two-dimensional disturbances in Blasius flow. In terms of computational effort, the approach of minimizing the shape factor is efficient. The optimality condition for each iteration in the optimization process is obtained after solving the boundary layer and corresponding adjoint equation once. The disadvantage lies in the fact that one does not take into account the disturbance growth in the optimization process, and consequently the effect of the control on the disturbance growth needs to be analyzed afterwards. Results here show that a control based on this objective function amplify instead of damp cross-flow modes in the region close to the leading edge of the wing. In this region, the optimal mass-flow distribution has a

positive sign, i.e., blowing occurs. The amplification of disturbances mean that the point of laminar-turbulent transition will move upstream and the laminar portion of the wing will decrease. Further, as the current way of implementing suction systems relies on pressure chambers, a region of blowing is not realizable.

Results are also presented for the optimal static pressure in a number of pressure chambers. These results depend on the choice of size, position and number of the chambers. However, it can be shown that the corresponding suction distributions are similar in magnitude compared to the result of the optimal suction distribution in a continuous control domain. This similarity increases as the number of pressure chambers is increased.

The magnitudes of the suction distributions presented in this paper are all of order $O(\text{Re}^{-1})$, which is within the range of validity of the boundary-layer equations. As Airiau *et al.*⁹ showed, for the suction rate of this order, the boundary-layer and Navier–Stokes calculations agreed well though the optimal mass flux experiences locally large streamwise variation.

ACKNOWLEDGMENTS

The useful discussion with C. Airiau and other colleagues, and financial support of the EU project (ALTTA Contract No. G4RD-CT-2000-00143) are gratefully acknowledged.

APPENDIX A: OPTIMAL CONTROL USING THE WALL MASS FLUX TO MINIMIZE THE DISTURBANCE KINETIC ENERGY

1. State equations

The boundary-layer equations for a viscous compressible flow over a swept wing with an infinite span are

$$\frac{1}{h_1} \frac{\partial(\rho U)}{\partial x^1} + \frac{\partial(\rho W)}{\partial x^3} = 0, \tag{A1}$$

$$\frac{\rho U}{h_1} \frac{\partial U}{\partial x^1} + \rho W \frac{\partial U}{\partial x^3} = -\frac{1}{h_1} \frac{dP_e}{dx^1} + \frac{1}{\text{Re}} \frac{\partial}{\partial x^3} \left(\mu \frac{\partial U}{\partial x^3} \right), \tag{A2}$$

$$\frac{\rho U}{h_1} \frac{\partial V}{\partial x^1} + \rho W \frac{\partial V}{\partial x^3} = \frac{1}{\text{Re}} \frac{\partial}{\partial x^3} \left(\mu \frac{\partial V}{\partial x^3} \right), \tag{A3}$$

$$\begin{aligned} c_p \frac{\rho U}{h_1} \frac{\partial T}{\partial x^1} + c_p \rho W \frac{\partial T}{\partial x^3} &= \frac{1}{\text{Re Pr}} \frac{\partial}{\partial x^3} \left(\kappa \frac{\partial T}{\partial x^3} \right) + (\gamma - 1) \frac{UM^2}{h_1} \frac{dP_e}{dx^1} \\ &+ (\gamma - 1) \frac{\mu M^2}{\text{Re}} \left[\left(\frac{\partial U}{\partial x^3} \right)^2 + \left(\frac{\partial V}{\partial x^3} \right)^2 \right]. \end{aligned} \tag{A4}$$

The parabolized stability equations are lengthy and here are given in a symbolic form

$$\mathcal{A}\hat{\mathbf{q}} + \mathcal{B} \frac{\partial \hat{\mathbf{q}}}{\partial x^3} + \mathcal{C} \frac{\partial^2 \hat{\mathbf{q}}}{(\partial x^3)^2} + \mathcal{D} \frac{1}{h_1} \frac{\partial \hat{\mathbf{q}}}{\partial x^1} = 0, \tag{A5}$$

$$\int_0^{+\infty} \hat{\mathbf{q}}^H \frac{\partial \hat{\mathbf{q}}}{\partial x^1} dx^3 = 0, \quad \forall x^1 \in [X_0, X_1], \tag{A6}$$

where $\hat{\mathbf{q}} = (\hat{\rho}, \hat{u}, \hat{v}, \hat{w}, \hat{T})^T$. The coefficients of the 5×5 matrices \mathcal{A} , \mathcal{B} , \mathcal{C} , and \mathcal{D} are found in Pralits *et al.*²³ The corresponding boundary conditions are

$$W(x^1, 0) = W_w(x^1) \quad \forall x^1 \in \Gamma_c,$$

$$W(x^1, 0) = 0 \quad \forall x^1 \notin \Gamma_c,$$

$$\left[U, V, \frac{\partial T}{\partial x^3} \right] (x^1, 0) = [0, 0, 0] \quad \forall x^1 \in [X_S, X_1],$$

$$\lim_{x^3 \rightarrow +\infty} [U, V, T](x^1, x^3) = [U_e, V_e, T_e](x^1) \quad \forall x^1 \in [X_S, X_1],$$

$$[\hat{u}, \hat{v}, \hat{w}, \hat{T}](x^1, 0) = [0, 0, 0, 0] \quad \forall x^1 \in [X_0, X_1],$$

$$\lim_{x^3 \rightarrow +\infty} [\hat{u}, \hat{v}, \hat{w}, \hat{T}](x^1, x^3) = [0, 0, 0, 0] \quad \forall x^1 \in [X_0, X_1],$$

where variables with subscript w are evaluated at the wall, and subscript e at the boundary layer edge. The initial conditions are

$$\mathbf{Q}(X_S, x^3) = \mathbf{Q}_S(x^3) \quad \forall x^3 \in [0, +\infty),$$

$$\hat{\mathbf{q}}(X_0, x^3) = \hat{\mathbf{q}}_0(x^3) \quad \forall x^3 \in [0, +\infty),$$

where the solution of variables with subscript 0 is given by the local stability analysis, and subscript S by the solution at the stagnation line.

2. Adjoint equations

The adjoint of the boundary-layer equations are

$$\rho \frac{\partial(h_1 W^*)}{\partial x^3} - h_1 \rho \left(\frac{\partial U}{\partial x^3} U^* + \frac{\partial V}{\partial x^3} V^* + c_p \frac{\partial T}{\partial x^3} T^* \right) = F_w h_1, \tag{A7}$$

$$\begin{aligned} \frac{\partial(\rho U U^*)}{\partial x^1} + \frac{\partial(h_1 \rho W U^*)}{\partial x^3} &- \rho \left(\frac{\partial U}{\partial x^1} U^* + \frac{\partial V}{\partial x^1} V^* - \frac{\partial W^*}{\partial x^1} + c_p \frac{\partial T}{\partial x^1} T^* \right) + (\gamma - 1) \\ &\times M^2 \frac{dP_e}{dx^1} T^* - \frac{2(\gamma - 1)}{\text{Re}} M^2 \frac{\partial}{\partial x^3} \left(h_1 \mu \frac{\partial U}{\partial x^3} T^* \right) \\ &+ \frac{1}{\text{Re}} \frac{\partial}{\partial x^3} \left(\mu \frac{\partial(h_1 U^*)}{\partial x^3} \right) = F_U h_1, \end{aligned} \tag{A8}$$

$$\begin{aligned} \frac{\partial(\rho U V^*)}{\partial x^1} + \frac{\partial(h_1 \rho W V^*)}{\partial x_3} - \frac{2(\gamma - 1)}{\text{Re}} M^2 \frac{\partial}{\partial x^3} \left(h_1 \mu \frac{\partial V}{\partial x^3} T^* \right) \\ + \frac{1}{\text{Re}} \frac{\partial}{\partial x^3} \left(\mu \frac{\partial(h_1 V^*)}{\partial x^3} \right) = F_V h_1, \end{aligned} \tag{A9}$$

$$\begin{aligned} c_p \frac{\partial(\rho U T^*)}{\partial x^1} + c_p \frac{\partial(h_1 \rho W T^*)}{\partial x^3} \\ + \frac{\rho U}{T} \left(\frac{\partial U}{\partial x^1} U^* + \frac{\partial V}{\partial x^1} V^* - \frac{\partial W^*}{\partial x^1} + c_p \frac{\partial T}{\partial x^1} T^* \right) \\ + \frac{\kappa}{\text{Re Pr}} \frac{\partial^2(h_1 T^*)}{(\partial x^3)^2} + \frac{(\gamma - 1)}{\text{Re}} \end{aligned}$$

$$\begin{aligned} & \times M^2 \frac{d\mu}{dT} \left[\left(\frac{\partial U}{\partial x^3} \right)^2 + \left(\frac{\partial V}{\partial x^3} \right)^2 \right] T^* \\ & - \frac{1}{\text{Re}} \frac{d\mu}{dT} \left[\frac{\partial U}{\partial x^3} \frac{\partial(h_1 U^*)}{\partial x^3} + \frac{\partial V}{\partial x^3} \frac{\partial(h_1 V^*)}{\partial x^3} \right] = F_E h_1, \end{aligned} \quad (\text{A10})$$

where $F_E = (F_T + F_W W/T)h_1$, and F_W , F_U , F_V , F_T are found in Pralits.²⁷ The adjoint of the parabolized stability equations can be written as

$$\tilde{\mathcal{A}}\mathbf{q}^* + \tilde{\mathcal{B}} \frac{\partial \mathbf{q}^*}{\partial x^3} + \tilde{\mathcal{C}} \frac{\partial^2 \mathbf{q}^*}{(\partial x^3)^2} + \tilde{\mathcal{D}} \frac{1}{h_1} \frac{\partial \mathbf{q}^*}{\partial x^1} = S_p^*, \quad (\text{A11})$$

$$\begin{aligned} & \frac{\partial}{\partial x^1} \int_0^{+\infty} \mathbf{q}^{*H} \left(\frac{\partial \mathcal{A}}{\partial \alpha} + \frac{\partial \mathcal{B}}{\partial \alpha} \right) \tilde{\mathbf{q}} h_1 dx^3 \\ & = \begin{cases} 0 & \forall x^1 \notin [X_{ms}, X_{me}], \\ -i|\Theta|^2 \int_0^{+\infty} \tilde{\mathbf{q}}^H M \tilde{\mathbf{q}} h_1 dx^3 & \forall x^1 \in [X_{ms}, X_{me}], \end{cases} \end{aligned} \quad (\text{A12})$$

where

$$S_p^* = \begin{cases} -\bar{r}^* \frac{\partial \hat{\mathbf{q}}}{\partial x^1} - \frac{\partial(r^* \hat{\mathbf{q}})}{\partial x^1} & \forall x^1 \notin [X_{ms}, X_{me}], \\ -\bar{r}^* \frac{\partial \hat{\mathbf{q}}}{\partial x^1} - \frac{\partial(r^* \hat{\mathbf{q}})}{\partial x^1} + \xi M^H \hat{\mathbf{q}} |\Theta|^2 & \forall x^1 \in [X_{ms}, X_{me}], \end{cases}$$

and

$$\tilde{\mathcal{A}} = \mathcal{A}^H - \frac{\partial \mathcal{B}^H}{\partial x^3} - m_{13} \mathcal{B}^H + \frac{\partial^2 \mathcal{C}^H}{(\partial x^3)^2} + 2m_{13} \frac{\partial \mathcal{C}^H}{\partial x^3} - \frac{\partial \mathcal{D}^H}{\partial x^1},$$

$$\tilde{\mathcal{B}} = -\mathcal{B}^H + 2 \frac{\partial \mathcal{C}^H}{\partial x^3} + 2m_{13} \mathcal{C}^H,$$

$$\tilde{\mathcal{C}} = \mathcal{C}^H,$$

$$\tilde{\mathcal{D}} = -\mathcal{D}^H.$$

The vector $\mathbf{q}^* = (\rho^*, u^*, v^*, w^*, \theta^*)^T$, and the complete derivation of these equations is found in Pralits *et al.*²³ The above equations are subjected to the following boundary conditions:

$$[u^*, v^*, w^*, \theta^*](x^1, 0) = [0, 0, 0, 0] \quad \forall x^1 \in [X_0, X_1],$$

$$\lim_{x^3 \rightarrow +\infty} [u^*, v^*, w^*, \theta^*](x^1, x^3) = [0, 0, 0, 0] \quad \forall x^1 \in [X_0, X_1],$$

$$[U^*, V^*](x^1, 0) = [0, 0] \quad \forall x^1 \in [X_0, X_1],$$

$$\left[\frac{\kappa}{\text{Re Pr}} \frac{\partial(h_1 T^*)}{\partial x^3} + h_1 \rho c_p W T^* \right](x^1, 0) = 0 \quad \forall x^1 \in [X_0, X_1],$$

$$\lim_{x^3 \rightarrow +\infty} [U^*, V^*, W^*, T^*](x^1, x^3) = [0, 0, 0, 0]$$

$$\forall x^1 \in [X_0, X_1].$$

The initial conditions are

$$\mathbf{q}^*(X_1, x^3) = (1 - \xi) \mathbf{q}_1^*(x^3) \quad \forall x^3 \in [0, +\infty),$$

$$r^*(X_1) = (1 - \xi) r_1^* \quad \forall x^3 \in [0, +\infty),$$

$$\mathbf{Q}^*(X_1, x^3) = \mathbf{0} \quad \forall x^3 \in [0, +\infty),$$

with \mathbf{q}_1^* and r_1^* evaluated at $x^1 = X_1$ as

$$\mathbf{q}_1^* = |\Theta|^2 \mathcal{D}^+ (M - c_1 \mathcal{I}) \hat{\mathbf{q}}, \quad r_1^* = |\Theta|^2 c_1,$$

$$\bar{c}_1 = \frac{\int_0^\infty \left(h_1 \hat{\mathbf{q}}^H M \mathcal{D}^{+H} \left(\frac{\partial \mathcal{A}}{\partial \alpha} + \frac{\partial \mathcal{B}}{\partial \alpha} \right) \hat{\mathbf{q}} - i \hat{\mathbf{q}}^H M \hat{\mathbf{q}} \right) dx^3}{\int_0^\infty \hat{\mathbf{q}}^H \mathcal{D}^{+H} \left(\frac{\partial \mathcal{A}}{\partial \alpha} + \frac{\partial \mathcal{B}}{\partial \alpha} \right) \hat{\mathbf{q}} h_1 dx^3}, \quad (\text{A13})$$

where $\mathcal{D}^+ = (\mathcal{D}^H)^{-1}$.

3. Optimality condition

The optimality condition is

$$W_w^* = \begin{cases} -2\chi^* \dot{m}_w & \forall x^1 \in \Gamma_c, \\ 0 & \forall x^1 \notin \Gamma_c, \end{cases} \quad (\text{A14})$$

where

$$\chi^* = \left(\frac{1}{4E_C} \int_{X_{cs}}^{X_{ce}} W_w^{*2} h_1 dx^1 \right)^{1/2}.$$

APPENDIX B: OPTIMAL CONTROL USING THE WALL MASS FLUX TO MINIMIZE THE SHAPE FACTOR

1. State equations

The boundary layer equations are given by Eqs. (A1), (A2), (A3), and (A4) with corresponding boundary and initial conditions as given in Appendix A 1.

2. Adjoint equations

The adjoint boundary layer equations are given by Eqs. (A7), (A8), (A9), and (A10) where the component of the forcing $S_B^* = (F_W, F_U, F_V, F_E)$ are now

$$F_W = 0,$$

$$F_U = \frac{1}{\delta_2} \rho \cos(\phi) (1 + H_{12}(1 - 2U_{SL})) \frac{U_{e0}}{Q_e},$$

$$F_V = \frac{1}{\delta_2} \rho \sin(\phi) (1 + H_{12}(1 - 2U_{SL})) \frac{U_{e0}}{Q_e},$$

$$F_E = -\frac{1}{\delta_2} \frac{\rho}{T} U_{SL} (1 + H_{12}(1 - U_{SL})) \frac{T_{e0}}{T_e}.$$

The initial and boundary conditions are the ones given in Appendix A 2, except for free stream boundary conditions which are now given as

$$\lim_{x^3 \rightarrow +\infty} \left[\frac{\partial U^*}{\partial x^3}, \frac{\partial V^*}{\partial x^3}, W^*, \frac{\partial T^*}{\partial x^3} \right](x^1, x^3) = [0, 0, 0, 0]$$

$$\forall x^1 \in [X_0, X_1].$$

3. Optimality condition

The optimality condition is given by Eq. (A14).

APPENDIX C: OPTIMAL CONTROL USING PRESSURE CHAMBERS TO MINIMIZE THE DISTURBANCE KINETIC ENERGY

1. Relation between internal static pressure and mass flux

The relation between the pressure difference and suction velocity used here is taken from Bieler and Preist.¹⁷ It is based on measurements carried out in the framework of the ELFIN (European Laminar Flow INvestigation) program. In dimensionless form this formula is given as

$$\Delta P_j = P_e - P_{c_j} = \frac{C_1}{\rho_w} \dot{m}_w^2 + C_2 \frac{\mu_w}{\rho_w} \dot{m}_w,$$

where

$$C_1 = \frac{A}{2} \left(\frac{4\epsilon^2}{\pi} \right)^2, \quad C_2 = \frac{32B}{\text{Re}} \frac{4\epsilon^2}{\pi} \frac{L}{d^2}.$$

The porous plate has a thickness L and a hole diameter d at the surface. Due to manufacturing reasons the holes were slightly conical with an inner diameter D . The porosity is

given as $\pi/(4\epsilon^2)$, where ϵ is the ratio between the hole diameter on the surface and the distance between the holes.

It was found in experiments that the relationship between the suction velocity and pressure difference was non-linear and that adding a term due to dynamic pressure loss with an empirically obtained coefficient A gave a good agreement with experiments.¹⁷ The second term on the right-hand side of the formula is based on the Hagen–Poiseuille equation for pressure loss due to skin friction in a hole with parallel walls. The coefficient B is a function of the inner and outer hole diameters and serves as a correction due to the conical shape of the holes.

2. State equations

The boundary-layer equations are given by Eqs. (A1), (A2), (A3), and (A4) with corresponding initial conditions as given in Appendix A 1. All boundary conditions are the same as given in Appendix A 1, except for the wall normal mean velocity at the wall, which is now given by

$$W(x^1, 0) = \begin{cases} 0 & \forall x^1 \in [X_{cs_j}, X_{ce_j}], \\ -\frac{1}{2} \frac{C_2}{C_1} \frac{\mu_w}{\rho_w} + \sqrt{\left(\frac{1}{2} \frac{C_2}{C_1} \frac{\mu_w}{\rho_w} \right)^2 + \Delta P_j \frac{\rho_w}{C_1}} & \forall x^1 \in [X_{cs_j}, X_{ce_j}]. \end{cases}$$

The values used here for A , B , L , d , and ϵ are taken from Bieler and Preist.¹⁷ The parabolized stability equations are given by Eqs. (A5) and (A6) with corresponding boundary and initial conditions as given in Appendix A 1.

3. Adjoint equations

The adjoint parabolized stability equations are given by Eqs. (A11) and (A12) with corresponding boundary and initial conditions as given in Appendix A 2. The adjoint boundary layer equations are given by Eqs. (A7), (A8), (A9), and (A10) with corresponding initial conditions as given in Appendix A 2. All boundary conditions are the same as given in Appendix A 2, except for T^* at the wall, which is now given by

$$\left[\frac{\kappa}{\text{Re Pr}} \frac{\partial(h_1 T^*)}{\partial x^3} + h_1 \rho c_p W T^* \right] (x^1, 0) = \begin{cases} 0 & \forall x^1 \in [X_{cs_j}, X_{ce_j}], \\ K_j (W^* + 2\chi^* \dot{m}_w) & \forall x^1 \in [X_{cs_j}, X_{ce_j}], \end{cases}$$

where

$$K_j = \frac{\partial P_{c_j}}{\partial T_w} \bigg/ \frac{\partial P_{c_j}}{\partial \dot{m}_w},$$

and

$$\left. \begin{aligned} \frac{\partial P_{c_j}}{\partial T_w} &= \frac{1}{\rho_w T_w} C_1 \dot{m}_w^2 + C_2 \frac{1}{\rho_w} \left(\frac{\mu_w}{T_w} + \frac{d\mu_w}{dT_w} \right) \dot{m}_w \\ \frac{\partial P_{c_j}}{\partial \dot{m}_w} &= \frac{2C_1}{\rho_w} \dot{m}_w + C_2 \frac{\mu_w}{\rho_w} \end{aligned} \right\} \forall x^1 \in [X_{cs_j}, X_{ce_j}].$$

4. Optimality condition

We find

$$- \int_{X_{cs_j}}^{X_{ce_j}} (W_w^* + 2\chi_w^* \dot{m}_w) \left(\frac{\partial P_{c_j}}{\partial \dot{m}_w} \right)^{-1} h_1 dx^1 = 0, \quad j=1, \dots, K,$$

where

$$\chi^* = \left(\frac{1}{4E_C} \sum_{j=1}^K \int_{X_{csj}}^{X_{cej}} W_w^{*2} h_1 dx^1 \right)^{1/2}.$$

- ¹R. D. Joslin, "Overview of laminar flow control," Technical Report 1998-208705, NASA, Langley Research Center, Hampton, Virginia, October 1998.
- ²J. L. van Ingen, "A suggested semiempirical method for the calculation of the boundary layer transition region," Technical Report VTH-74, Department of Aeronautical Engineering, University of Delft, 1956.
- ³A. M. O. Smith and N. Gamberoni, "Transition, pressure gradient and stability theory," Technical Report ES 26388, Douglas Aircraft Co., 1956.
- ⁴H. Schlichting, "Die beeinflussung der grenzschicht durch absaugung und ausblasen," *Jb. dt. Adad. d. Luftfahrtforschung*, 90–108, 1943/44.
- ⁵D. C. Hill, "Inverse design for laminar three-dimensional boundary layers," *Bull. Am. Phys. Soc.* **42**, 2120 (1997).
- ⁶P. Balakumar and P. Hall, "Optimum suction distribution for transition prediction," *Theor. Comput. Fluid Dyn.* **13**, 1 (1999).
- ⁷P. Cathalifaud and P. Luchini, "Algebraic growth in a boundary layer: optimal control by blowing and suction at the wall," *Eur. J. Mech. B/Fluids* **19**, 469 (2000).
- ⁸J. O. Pralits, A. Hanifi, and D. S. Henningson, "Adjoint-based optimization of steady suction for disturbance control in incompressible flows," *J. Fluid Mech.* **467**, 129 (2002).
- ⁹C. Airiau, A. Bottaro, S. Walther, and D. Legendre, "A methodology for optimal laminar flow control: Application to the damping of Tollmien–Schlichting waves in a boundary layer," *Phys. Fluids* **15**, 1131 (2003).
- ¹⁰M. S. Mughal, "Active control of instabilities in three-dimensional compressible flows," *Theor. Comput. Fluid Dyn.* **12**, 195 (1998).
- ¹¹S. Walther, C. Airiau, and A. Bottaro, "Optimal control of Tollmien–Schlichting waves in a developing boundary layer," *Phys. Fluids* **13**, 2087 (2001).
- ¹²M. Högberg and D. S. Henningson, "Linear optimal control applied to instabilities in spatially developing boundary layers," *J. Fluid Mech.* **470**, 151 (2002).
- ¹³T. R. Bewley, "Flow control: new challenges for a new renaissance," *Prog. Aerosp. Sci.* **37**, 21 (2001).
- ¹⁴J. Reneaux and A. Blanchard, "The design and testing of an airfoil with hybrid laminar flow control," First European Forum on Laminar Flow Technology, Hamburg, 1992, pp. 164–174.
- ¹⁵J. E. Ellis and D. I. A. Poll, "Laminar and laminarizing boundary layers by suction through perforated plates," Second European Forum on Laminar Flow Technology, Bordeaux, 1996, pp. 8.17–8.26.
- ¹⁶K. Preist and B. Paluch, "Design specification and inspection of perforated panels for hlf suction systems," Second European Forum on Laminar Flow Technology, Bordeaux, 1996, pp. 6.20–6.34.
- ¹⁷H. Bieler and J. Preist, "Hlfc for commercial aircraft," First European Forum on Laminar Flow Technology, Hamburg, 1992, pp. 193–199.
- ¹⁸C. J. Atkin, "New aerodynamic approach to suction system design," in *CEAS/DragNet European Drag Reduction Conference*, edited by P. Thiede, Potsdam, Germany (Springer, Berlin, 2000).
- ¹⁹F. P. Bertolotti, Th. Herbert, and S. P. Spalart, "Linear and nonlinear stability of the Blasius boundary layer," *J. Fluid Mech.* **242**, 441 (1992).
- ²⁰M. R. Malik and P. Balakumar, "Nonparallel stability of rotating disk flow using pse," in *Instability, Transition and Turbulence*, edited by M. Y. Hussaini *et al.* (Springer, New York, 1992), pp. 168–180.
- ²¹M. Simen, "Local and non-local stability theory of spatially varying flows," in *Instability, Transition and Turbulence*, edited by M. Hussaini *et al.* (Springer, New York, 1992), pp. 181–201.
- ²²T. Herbert, "Parabolized stability equations," *Annu. Rev. Fluid Mech.* **29**, 245 (1997).
- ²³J. O. Pralits, C. Airiau, A. Hanifi, and D. S. Henningson, "Sensitivity analysis using adjoint parabolized stability equations for compressible flows," *Flow, Turbul. Combust.* **65**, 321 (2000).
- ²⁴A. Hanifi, D. S. Henningson, S. Hein, M. Bertolotti, and F. P. Simen, "Linear non-local instability analysis—the linear nolot code," FFA TN, 1994–54, 1994.
- ²⁵A. Hanifi, P. J. Schmid, and D. S. Henningson, "Transient growth in compressible boundary layer flow," *Phys. Fluids* **8**, 826 (1996).
- ²⁶M. D. Gunzburger, "Introduction into mathematical aspects of flow control and optimization," Von Karman Institute for Fluid Dynamics, Lecture Series 1997-05, Inverse Design and Optimization Methods, 1997.
- ²⁷J. O. Pralits, "Towards optimal design of vehicles with low drag: Applications to sensitivity analysis and optimal control," Licentiate thesis KTH/MEK/TR-01/07, Royal Institute of Technology, SE-172 90 Stockholm, Sweden, 2001.
- ²⁸C. Zhu, R. H. Byrd, P. Lu, and J. Nocedal, "L-bfgs-b: Fortran subroutines for large scale bound constrained optimization," Technical Report NAM-11, EECS Department, Northwestern University, 1994.
- ²⁹R. H. Byrd, P. Lu, J. Nocedal, and C. Zhu, "A limited memory algorithm for bound constrained optimization," *SIAM J. Sci. Comput. (USA)* **16**, 1190 (1995).